International Journal of Remote Sensing

ISSN: 0143-1161 (Print) 1366-5901 (Online) Journal homepage: www.tandfonline.com/journals/tres20

Sub-pixel detection of dominant grass evolutionary lineages at four sites across the Great Plains, U.S. using hyperspectral data

Ryan Slapikas, Ryan C. Donnelly, Jesse B. Nippert & Stephanie Pau

To cite this article: Ryan Slapikas, Ryan C. Donnelly, Jesse B. Nippert & Stephanie Pau (26 Nov 2025): Sub-pixel detection of dominant grass evolutionary lineages at four sites across the Great Plains, U.S. using hyperspectral data, International Journal of Remote Sensing, DOI: 10.1080/01431161.2025.2593712

To link to this article: https://doi.org/10.1080/01431161.2025.2593712

INTERNATIONAL JOURNAL OF REMOTE SENSING
https://doi.org/10.1080/01431161.2025.2593712

Taylor & Francis
Taylor & Francis Group

Sub-pixel detection of dominant grass evolutionary lineages at four sites across the Great Plains, U.S. using hyperspectral data

Ryan Slapikas [a], Ryan C. Donnelly [b], Jesse B. Nippert [b] and Stephanie Pau [c,d]

[a]Department of Geography, Florida State University, Tallahassee, FL, USA; [b]Division of Biology, Kansas State University, Manhattan, KS, USA; [c]Department of Geography, University of California, Berkeley, CA, USA; [d]Department of Environmental Science, Policy, and Management, University of California, Berkeley, CA, USA

ABSTRACT

Grasslands exhibit high taxonomic and functional diversity, particularly at fine spatial scales, posing challenges for remote sensing due to patchiness and species turnover. The spatial resolution of most remote sensing platforms often exceeds the size of homogeneous grassland patches, resulting in mixed pixels that hinder vegetation mapping. To address this, we applied Multiple Endmember Spectral Mixture Analysis (MESMA) to high-resolution (1 m^2) hyperspectral imagery from the NEON Airborne Observatory Platform (AOP) to assess the predictive accuracies of fractional cover and dominance of four major grass evolutionary lineages, Andropogoneae, Panicoideae, Chloridoideae, and Pooideae, across four U.S. Great Plains grasslands. MESMA performance was evaluated using different endmember selection strategies, including leaf- vs. plot-level spectral endmembers and site-specific vs. multiple-site endmembers. Overall classification accuracy reached ~90% (Matthews Correlation Coefficient ~0.84) using optimal endmember combinations. While no single approach was universally superior, in general, leaf-level endmembers from focal sites and plot-level endmembers aggregated across all sites yielded higher overall accuracies. These results demonstrate that plot-level endmembers are more transferable across sites compared to leaf-level endmembers. Our results furthermore demonstrate that incorporating information about evolutionary relatedness can improve spectral unmixing results. This study advances sub-pixel mapping of grassland composition, offering insights for ecological modelling, land change prediction, and assessing grassland responses to environmental change and community composition.

ARTICLE HISTORY
Received 9 April 2025
Accepted 9 November 2025

KEYWORDS
Biodiversity; evolutionary lineages; imaging spectroscopy

1. Introduction

Grasslands are among some of the most diverse ecosystems at small spatial extents (Wilson et al. 2012). In addition to being taxonomically and functionally diverse, they can be extremely patchy with high species turnover at varying scales. Accurately mapping

CONTACT Ryan Slapikas res09e@fsu.edu Department of Geography, Florida State University, 113 Collegiate Loop, Tallahassee, FL 32306, USA

Supplemental data for this article can be accessed online at https://doi.org/10.1080/01431161.2025.2593712

grass and grassland distribution with remote sensing frequently means confronting mixed pixels, when a pixel contains multiple subjects of interest (Pazúr et al. 2022). This is because the size of homogenous grassland patches is often exceeded by the size of the pixel of most remote sensing platforms (Gholizadeh et al. 2019, 2022; Lopatin et al. 2017; Van Cleemput et al. 2018). Such variation complicates remote sensing mapping efforts, which are critical to understanding the distribution of grasses and grasslands across large spatial extents and how they will respond to environmental change.

Spectral Mixture Analysis or SMA is a technique that determines the percentage of each subject or class within a heterogeneous pixel (Adams, Smith, and Johnson 1986). SMA is employed when the spatial resolution is larger than the object of interest. It allows for sub-pixel analysis, enabling the identification of pure sub-pixel signatures and analysing sub-pixel components to match the object or component of interest. SMA uses a combination of pure spectra of different surfaces referred to as endmembers (Adams, Smith, and Johnson 1986). SMA approaches are reliant on the availability of appropriate, representative endmembers (Tompkins et al. 1997). Using endmembers that are not representative of their respective features decreases performance (Song 2005). If endmembers are too similar and correlated with one another, accuracy declines significantly (Gong and Zhang 1999). Such similarity may be expected when utilizing lower resolution imagery to study grasslands as high inherent heterogeneity may result in the inadvertent selection of impure endmembers.

Methods for identifying the number and type of endmembers vary and can include different combinations of spectral endmembers from various sources and classes (Radeloff, Mladenoff, and Boyce 1999; Roberts et al. 1998; Smith et al. 1990; Wessman, Bateson, and Benning 1997; C. Wu and Murray 2003). Endmembers can be sourced from remotely sensed imagery or from spectral libraries of measurements recorded either in the field or the laboratory. For remote sensing of vegetation, leaf-level endmembers from spectral libraries are considered pure spectra without any canopy or illumination effects that may be location- or site-specific and thus can be applied to images where that species is known to occur. However, previous studies have underscored the benefits of using image endmembers with matching spatial scales for a number of reasons (Asner and Heidebrecht 2002; Kuemmerle, Röder, and Hill 2006; Rashed et al. 2003). Leaf-level endmembers from a spectral library may miss spectral complexities of plant canopies and illumination effects within heterogeneous landscapes and result in significant fractional estimate error (Somers et al. 2011). Factors such as solar zenith angle, sensor viewing direction, and canopy structure can contribute to variations in reflectance (Goodin, Gao, and Henebry 2004; Ranson et al. 1985). Furthermore, particularly in open grassy ecosystems, effects of soil reflectance are important to consider. Gholizadeh et al. (2018) demonstrated the importance of soil background effects in mapping grassland diversity at fine scales. They used spectral unmixing of hyperspectral imagery to derive soil percent cover fraction in pixels, which improved relationships between species diversity and spectral diversity. Thus, spectral endmembers taken in field conditions, at a spatial resolution that captures canopies instead of individual leaves (i.e. 'plot-level' spectra), may lead to more accurate SMA. While the collection of plot-level spectra, especially those taken during concurrent temporal timeframes (e.g. same season, month, or week) as imagery collection may provide spatially and temporally matched spectral signatures, it is time-consuming and often impractical to collect spectral endmembers in the field. If leaf

endmembers result in high predictive mapping accuracy, they can alleviate the need for time-consuming plot data.

Mapping grass functional groups is a precursor to important developments such as estimating grassland productivity and detecting grassland compositional change (Ali et al. 2016; Anderegg et al. 2022; Guerini Filho, Kuplich, and Quadros 2020; Hicke et al. 2002; Psomas et al. 2011; Smit, Metzger, and Ewert 2008; Xu et al. 2008). While the use of hyperspectral imagery has focused on mapping species diversity, species composition and functional identity may be key to understanding the relationship between grassland diversity and spectral diversity due to the sensitivity of spectra to structural and biochemical properties rather than species diversity per se (Asner and Martin 2011; Gholizadeh et al. 2019; Kothari and Schweiger 2022; Van Cleemput, Adler, and Suding 2023).

Across the Great Plains of the U.S., mapping grass distributions has commonly focused on large biogeographic gradients in species that utilize either the C_3 or C_4 photosynthetic pathways, with C_3 grasses dominant in cool wet environments and C_4 grasses dominant in warmer and wetter climates (Lehmann et al. 2019; Paruelo and Lauenroth 1996; Still et al. 2003). However, inaccuracies in predicting grassland distribution and productivity in vegetation models may be due to a lack of information on grass traits beyond photosynthetic pathway (Still, Cotton, and Griffith 2019). Photosynthetic pathway alone misses important trait diversity of grasses, which recent work has shown is better captured by evolutionary lineages and should underlie spectral reflectance (Donnelly et al. 2023; Pau et al. 2025). Using leaf-level hyperspectral reflectance of 43 grass species, Slapikas et al. (2024) predicted grass evolutionary lineages with very high accuracy (>90%). While these leaf-level spectra were able to discriminate grass evolutionary lineages, it is unclear if plot-level endmembers would perform better when applied to image unmixing for mapping purposes. The importance of identifying endmembers using data collected at the leaf-scale or using data that captures field conditions remains unknown.

Here, we applied SMA approaches, specifically Multiple Endmember Spectral Mixture Analysis (MESMA), to high-spatial resolution National Ecological Observatory Network (NEON) Airborne Observatory Platform (AOP) imagery with 1 m^2 resolution pixels of varying grass composition. We sought to compare the accuracies of different endmember selections in predicting the fine-scale composition of grass evolutionary lineages in mixed pixels across four grassland sites in the Great Plains region of the U.S.. Our objectives for this work are: 1) to use MESMA techniques to predict the fractional percentage and dominance within a 1 m^2 pixel of grass evolutionary lineages at multiple sites, modelled separately, across the Great Plains, U.S., 2) compare MESMA accuracies at each site using leaf-level spectral endmembers vs. plot-level spectral endmembers, and 3) compare MESMA accuracies at each site using geographically widespread spectral endmembers vs. endmembers from the focal site only (i.e. the site being modelled).

2. Methods

2.1. Study sites

Field sampling was conducted at four sites across the Great Plains of the United States: Konza Prairie Biological Station (KONZ) in the Flint Hills region of Kansas, the Colorado Plains Experimental Range (CPER) in the western Great Plains, the Chase

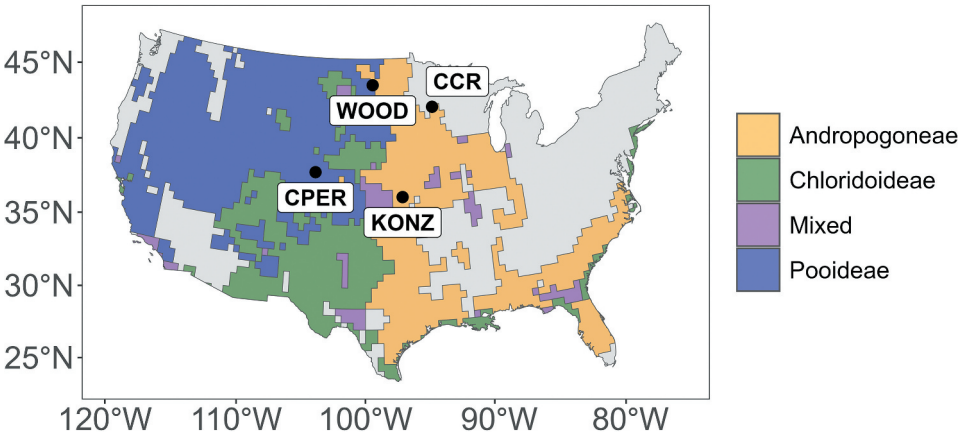

Figure 1. Our four study sites span a broad environmental gradient and are dominated by different grass evolutionary lineages, however these lineages also co-occur at fine scales. Colorado Plains Experimental Range (CPER; mean annual temperature (MAT) = 8.6°C, mean annual precipitation (MAP) = 344.2 mm), Konza Prairie (KONZ; MAT = 12.4°C, MAP = 870 mm), Cedar Creek Ecosystem Reserve (CCR; MAT = 6.7°C, MAP = 660.4 mm), and Chase Lake National Wildlife Refuge (WOOD; MAT = 4.9°C, MAP = 495 mm).

Lake National Wildlife Refuge (WOOD) east of Woodworth, North Dakota, and the Cedar Creek Ecosystem Reserve in central Minnesota (CCR) (Figure 1). These sites were chosen for their grass dominated ecosystems, to cover a wide environmental gradient, and the fact that each site is characterized by a distinct dominant grass lineage. KONZ is almost 3,500 hectares in size and managed by Kansas State University. The primary vegetation at Konza is a native tallgrass prairie, dominated by C_4 grasses, with managed burns and herbivore grazing. CPER is a roughly 6,500-hectare site managed by the U.S. Department of Agricultural Research Service. Dominant vegetation at CPER is a shortgrass steppe that is moderately grazed. The WOOD site is just over 1,000 hectares and is managed by the U.S. Fish and Wildlife Service and the U.S. Geological Survey. Prairie grasslands and croplands dominate this site, and light cattle grazing and prescribed burns are used. CCR is a 2,200-hectare reserve managed by the University of Minnesota. It contains coniferous forest, deciduous forest, and tallgrass prairie, which are managed using prescribed burns and grazing.

2.2. Data collection

2.2.1. Field data collection

Ground-based spectral measurements were conducted in the field during periods of peak greenness and on the same dates or within a few days of NEON AOP flyovers to mitigate potential phenological disparities. Ground sampling occurred 8–14 July 2020 (KONZ), 6–8 June 2021 (CPER), 11–14 June 2021 (WOOD), and 20–26 June 2022 (CCR). Field measurements were always recorded on days with low cloud cover, between the hours of 10am to 2pm. The Malveryn/ASD FieldSpec 4 Hi-Res NG Spectroradiometer, a portable

Table 1. Grass species grouped by evolutionary lineage are used as spectral endmembers. Species are organized according to their respective endmembers (Andropogoneae, Chloridoideae, Panicoideae, and Pooideae), which represent dominant grass evolutionary lineages. These groups served as endmembers in spectral unmixing analyses to characterize lineage-level reflectance patterns.

Dominant grass lineages	Photosynthetic type	Species
Andropogoneae	C_4	*Andropogon gerardii, Bothriochloa bladhii, Bothriochloa ischaemum, Bothriochloa laguroides, Schizachyrium scoparium, Sorghastrum nutans, Sorghum halepense, Tripsacum dactyloides*
Chloridoideae	C_4	*Bouteloua curtipendula, Bouteloua dactyloides, Bouteloua gracilis, Chloris verticillata, Eleusine indica, Eragrostis cilianensis, Muhlenbergia cuspidata, Muhlenbergia frondosa, Schedonnardus paniculatus, Spartina pectinata, Sporobolus compositus, Sporobolus heterolepis, Sporobolus vaginiflorus*
Panicoideae	C_3	*Dichanthelium leibergii, Dichanthelium oligosanthes, Dichanthelium perlongum, Dichanthelium praecocius*
	C_4	*Digitaria cognata, Echinochloa muricata, Hopia obtusa, Panicum virgatum, Paspalum setaceum, Setaria pumila, Setaria viridis*
Pooideae	C_3	*Agropyron cristatum, Agrostis gigantea, Bromus inermis, Bromus pubescens, Bromus tectorum, Diarrhena obovata, Elymus canadensis, Elymus elymoides, Elymus repens, Elymus smithii, Elymus villosus, Elymus virginicus, Glyceria striata, Hesperostipa comata, Hesperostipa spartea, Koeleria macrantha, Nassella viridula, Oryzopsis hymenoides, Phalaris arundinacea, Phleum pratense, Poa pratensis, Vulpia octoflora*

spectrometer designed for usage in both field campaigns and laboratory settings, was used to collect spectral measurements at both the leaf and the plot scale. The FieldSpec 4 Hi-Res NG has a spectral range from 350 to 2500 nm with a sampling interval of 1.4–2 nm for 350–1000 nm and 1001–2500 nm, respectively. The spectroradiometer was set to 25 internal repetitions. The data were corrected for spectral discontinuities between the three spectroradiometer sensors using a jump correction as in Dorigo, Bachmann, and Heldens (2006).

A total of 54 grass species (Table 1), with five to eight replicates per species, were collected across the four sites. These 54 grass species were classified into four dominant lineages: Andropogoneae (which falls within the Panicoideae subfamily), remaining Panicoideae (species excluding Andropogoneae, which we henceforth refer to as 'Panicoideae' for simplicity), Chloridoideae, and Pooideae. The Andropogoneae tribe is recognized as a globally dominant grass lineage due to its widespread distribution and ecological significance. It is typically considered separately because it represents an independently evolved C_4 lineage with distinct biogeographical patterns and functional traits that differentiate it from other Panicoideae (Donnelly et al. 2023; Griffith et al. 2020). Because we did not want to exclude the remaining Panicoideae species, we classified those as a separate group and refer to that group as 'Panicoideae' although it excludes Andropogoneae species. Andropogoneae was represented by eight species, Chloridoideae was represented by 13 species, Panicoideae was represented by 11 species, and Pooideae was represented by 22 species.

2.2.1.1. Leaf spectral endmembers. Five to eight fresh leaf spectra from 54 grass species collected across all sites were measured using a leaf contact probe attachment (Slapikas et al. 2024). Leaves collected from the field were stored in a cooler with wet paper towels, and spectra were measured from fresh leaves within a 2-hr window of field sampling. A standard white reference built into the leaf clip (ASD Leaf Clip Version 2) was

measured for calibration before each species was measured and at 10-min intervals (Hellmann et al. 2015). Leaf sampling intensity was contingent upon leaf area; if a single leaf did not adequately cover the black background on the contact probe, multiple leaves were arranged adjacent to each other with their adaxial side facing the sensor (Slapikas et al. 2024).

The 54 grass species for leaf-level endmembers were chosen by first reviewing species lists and publicly available plot data to create rank abundance curves. We then targeted sampling of the most dominant species at each site. We additionally targeted species that occurred across multiple sites even when they were not dominant, as well as species that were representative of dominant lineages.

2.2.1.2. Plot spectral endmembers and ground validation data. We recorded spectral reflectance of 1 m^2 plots and associated species composition along multiple transect lines at each site (Supplementary Materials Figure S1). Each transect was 100 m in length. Beginning at 0 m, 1 m^2 quadrats were placed along the transect line, alternating sides every 10 m, for a total of 10 quadrats per transect. The spectral signature of each 1 m^2 plot was collected eight times using the portable spectroradiometer, which was later averaged to generate an average spectrum for each plot. The fore-optic lens inside the pistol grip, which has a field of view of 25 degrees, was held from the centre of each quadrat at a height of ~2 m to collect the spectra of the 1 m^2 plot. A standard white reference was used to generate a white reference spectrum before every plot measurement and at 10-min intervals (Hellmann et al. 2015). The percentage cover of all plant species greater than 5% within each 1 m^2 plot was recorded as well as overall plant species richness (Table 2). A total of 43 transects across all sites, generally 7–12 transects at each site, resulted in 430 1 m^2 plot measurements total. The latitudinal and longitudinal coordinates of the plot's centre were recorded using a GPS unit (Trimble R1 Integrated GNSS system, Trimble, Sunnyvale, CA, U.S.A.) with a location accuracy of 1–3 m.

The spectral library and endmembers were scaled to the same wavelength and spectral bands as the NEON AOP data. This scaling required reducing the data dimensions from 2,151 bands to 426 bands using the 'hsdar' package (Lehnert et al. 2019) in R.

Table 2. Representation of each lineage at each site.

Site	Lineage	Number of plots with lineage present	Range of % cover of lineage in 1 m^2 plots
KONZ	Andropogoneae	74	20–80%
	Chloridoideae	5	20–25%
	Panicoideae	3	20–40%
	Pooideae	3	5%
CPER	Andropogoneae	NA	NA
	Chloridoideae	33	20–45%
	Panicoideae	NA	NA
	Pooideae	30	20–90%
WOOD	Andropogoneae	5	25–40%
	Chloridoideae	2	5–12%
	Panicoideae	NA	NA
CCR	Andropogoneae	61	20–90%
	Chloridoideae	NA	NA
	Panicoideae	5	20–30%
	Pooideae	24	20–45%

2.2.2. Imagery collection and pre-processing

Three of our study sites, KONZ, CPER, and WOOD, are National Ecological Observatory Network (NEON) sites with publicly available hyperspectral and LiDAR imagery from the Airborne Observation Platform (AOP) provided at 1 m^2 spatial resolution. NEON's AOP is a multifunctional system equipped with three remote sensing instruments tailored for hyperspectral, multispectral, and LiDAR imaging (Kampe et al. 2010). The Imaging Spectrometer (NIS) records data in 426 bands from 380 to 2510 nm at 5 nm intervals. We downloaded NEON's fully orthorectified surface reflectance data (DP3.30006.001; accessed 5 July 2023) and LiDAR-derived Ecosystem Structure Canopy Height Model (CHM) (DP3.30015.001; accessed 5 July 2023) for all four of the sites. NEON produces the Ecosystem Structure CHM from LiDAR point cloud data as a continuous surface representing the height at the top of the canopy (m). We contracted Battelle/NEON to conduct AOP flights on 27 June 2022 and 29 June 2022 collecting LiDAR, imaging spectroscopy, and high-resolution camera imagery, and they produced AOP data products comparable to other NEON sites. NEON collected all AOP data within 1 week of our field sampling at all sites.

We used the NEON CHM to mask out non-grass dominated areas in the AOP imagery that had CHM over 2 m. We used orthorectified surface reflectance data and processed the data performing Bidirectional Reflectance Distribution Function (BRDF) correction to account for pronounced cross-track gradients. We used the 'HyTools' Python library to correct BRDF (Chlus 2023). We also removed the water absorption features (1330–1430 nm and 1800–1960 nm) and spectral ends (<400 nm and >2400 nm) due to low signal-to-noise ratios. Additionally, we filtered pixels with near-infrared (NIR) reflectance ≥20% and Normalized Difference Vegetation Index (NDVI) ≥0.5 to remove pixels with a large proportion of bareground, shadows, or other contaminants to well-lit vegetation pixels (Pau et al. 2022).

2.3. Analysis

2.3.1. Spectral endmember library creation and optimization

We used a leaf-level spectral library of 54 grass species from Slapikas et al. (2024; Figure 2) as well as a newly developed spectral library of 430 plot-level spectra from sampling at our four grassland sites (Tables 1 and 2). The two spectral libraries were applied to MESMA separately in leaf-level models or plot-level models. For each separate spectral library (i.e. leaf or plot), we generated spectral endmembers for each lineage using (1) reflectance collected from only the focal site (i.e. leaves or plots from the site being modelled) or (2) reflectance collected from all sites (i.e. leaves or plots from all of our study sites averaged for each lineage and applied to the site being modelled). We calculated leaf-level spectra for each species using mean reflectance values from all replicates, which were then aggregated to leaf-level lineage endmembers using the mean reflectance values for all species in each lineage. For plot-level endmembers for both focal-site and all-sites libraries, we used the plot with the highest % cover of each lineage at each site (Table 2). We also used the Pixel Purity Index (PPI; Boardman, Kruse, and Green 1995; Chang, Wu, and Chen 2009), which selected the same plots as endmembers as simply using the plot with the highest % cover of each lineage. We converted each plot spectra recorded from the

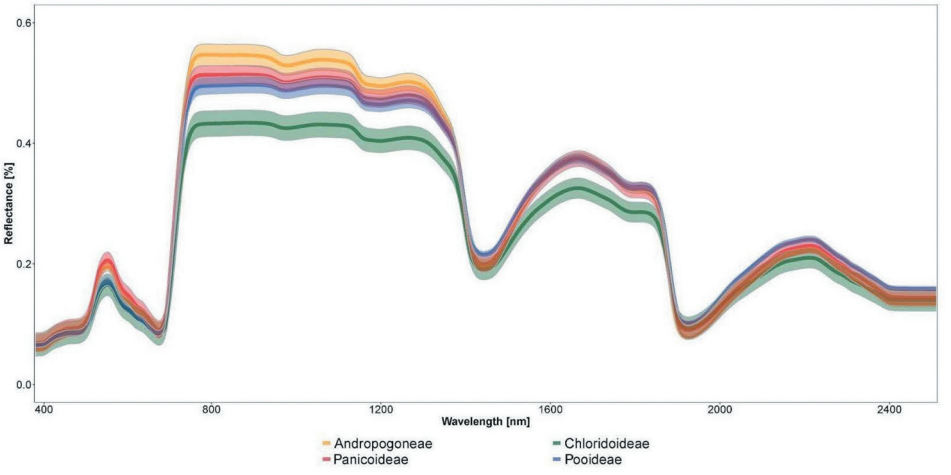

Figure 2. Leaf-level spectral endmembers used in Multiple Endmember Spectral Mixture Analysis (MESMA). The shaded regions represent ±2 standard deviations around the mean reflectance for each lineage, shown in the corresponding transparent colour. Remaining Panicoideae (species excluding Andropogoneae) we refer to as simply Panicoideae for simplicity.

field into a simulated pixel. Then, the PPI was used to identify endmember candidates for each lineage (all plots with that lineage present were used and this was repeated for each lineage at each site) by projecting each plot's spectra onto random unit vectors ('skewers'). Plot spectra towards extremes of each vector the most times, i.e. those with the highest PPI scores, were considered the most pure endmembers for each lineage.

Although we used an NDVI and NIR threshold to filter out potential bareground, shadows, and other unvegetated pixels in the AOP imagery (details above under 'Imagery collection and pre-processing'), we created bareground spectral endmembers derived from our plots into the MESMA process. Bareground endmembers were only used in our models of fractional percentage because there was essentially no bareground visible in plots used for our dominance models. These endmembers were used to account for pixels in the imagery that potentially included bareground, allowing for improved discrimination between vegetation and non-vegetated surfaces. The inclusion of bareground spectra can help mitigate classification errors and refine fractional abundance estimates in areas where soil exposure is present (Jacquemoud, Baret, and Hanocq 1992). The bareground endmember was based on the ground-truth plot with the highest percent cover of bareground across all the sites when applying endmembers aggregated across all sites. When endmembers from only focal sites were used, the plot with the highest percent cover of bareground at each site was selected as the bareground endmember.

2.3.2. Spectral unmixing

Multiple Endmember Spectral Mixture Analysis (MESMA) is an advanced type of linear SMA. Individual pixels are modelled independently with different

combinations of endmembers (Fernández-Guisuraga, Calvo, and Suárez-Seoane 2020; Fernández-Manso, Quintano, and Roberts 2012; Roberts et al. 1992, 1998). This contrasts with SMA in which individual pixels are modelled using the same combination of endmembers. MESMA is often used in land cover classifications, particularly when pixels are of a moderate resolution or lower, but the technique has also been applied to mapping dominant grassland species (e.g. Lopatin et al. 2017). We selected MESMA because the technique is particularly adept at managing the spectral signatures present in heterogeneous vegetation communities such as grasslands, where multiple endmembers contribute to the observed reflectance spectra (Y. He, Guo, and Wilmshurst 2006; Rossi and Gholizadeh 2023; J. Wu et al. 2023).

Leveraging our spectral libraries, we applied MESMA to predict both the dominant lineage and the fractional abundance (e.g. percentage) of each lineage within a pixel. The initial aim of using Spectral Mixture Analysis (SMA) was to assess how much representation of each endmember was present in the original data. However, an issue that arises with linear SMA is the fractional error when too few spectral endmembers are used within the model. MESMA is an extension of SMA and accounts for this issue of within-endmember variability. We performed MESMA using a non-negative least squares (NNLS) regression, which employs a sequential coordinate-wise algorithm (SCA) (Franc, Hlaváč, and Navara 2005), with the 'RStoolbox' package in R. The NNLS regression estimates the fractional cover of each endmember within a pixel. Each pixel spectrum is modelled as a linear combination of endmember spectra, subject to the constraints that the coefficients must be non-negative and sum up to ≤1. The primary parameters estimated by the NNLS regression are the fractional abundances (regression coefficients) for each selected endmember (e.g. Andropogoneae, Chloridoideae, Panicoideae, Pooideae, and bareground). Two additional parameters are available, which are the residual error term and user-defined constraints that include the sum-to-one condition and the maximum number of endmembers per pixel.

We applied MESMA to predict grass lineages in 1 m^2 AOP pixels using four approaches, both comparing leaf vs. plot-level endmembers and comparing all available endmembers vs. only focal site endmembers. First, we classified AOP pixels into their fractional cover of each grass lineage (Andropogoneae, Panicoideae, Chloridoideae, and Pooideae) using MESMA. For each site, we used linear regressions to assess the accuracy of predicted fractional cover. We compared predictive accuracies using models that did and did not include subfamily identity as an additional predictor in our models. Second, we used a minimum threshold of at least 30% cover and then classified each pixel to the most dominant lineage relative to other lineages present in ground-truth validation plots (i.e. pixels were classified as the lineage with the highest percent cover). We chose a minimum threshold of at least 30% because it was >¼ the size of the 1-m pixel (i.e. visually and ecologically dominant). The 30% cut-off operationalized dominance by reducing sensitivity to the inclusion of multiple lineages with potentially similar % cover. Through trial and error, we determined that a minimum of 30% cover was the lowest threshold that resulted in the highest classification accuracy. We evaluated the accuracy of dominance classifications using the Matthews Correlation Coefficient (MCC) rather than Cohen's Kappa, due to well-documented limitations of Kappa in providing meaningful or interpretable improvements to accuracy assessment (Foody 2020; Olofsson, Gilmore, and

Millones 2011). We assessed accuracy based on the dominant lineage classified within each AOP pixel using standard confusion matrix outputs. We calculated these accuracies for each of the four approaches we utilized (leaf-level across all sites, leaf-level from a single focal site, plot-level across all sites, plot-level from a single focal site). For both fractional cover and dominance predictions, we used percent cover values (of lineages and bareground) from 1 m^2 plots directly observed from the field at each site as validation plots, using GPS to geolocate the AOP pixel that corresponded to our 1 m^2 plot (see details above under 'Plot spectral endmembers and ground validation').

3. Results

3.1. Sub-pixel classification

The fractional coverage predictions using MESMA, with subfamily included as an additional covariate, showed improved performance when utilizing leaf-level endmembers from all sites or plot-level endmembers from the focal site, compared to other approaches (leaf-level endmembers from the focal site or plot-level endmembers from all sites) (Table 3). All unmixing models of fractional cover included a bareground endmember (see Figure S2 and Figure S3 in Supplementary Materials for confusion matrices). For the plot-level endmembers from the focal site approach, KONZ had the lowest RMSE of 16.46 and an R^2 of 0.87, whereas not including subfamily as an additional covariate the RMSE increased to 33.69 and the R^2 decreased to 0.44. CCR exhibited the highest RMSE of 26.59 and an R^2 of 0.53 with subfamily included and without had an RMSE of 38.64 and an R^2 of 0.01. Using leaf-level endmembers from all sites, R^2 values were generally higher than those observed using leaf-level endmembers from only the focal site, with the exception of CPER, where the focal site approach produced a higher R^2. Among all sites, predictions at WOOD had the lowest

Table 3. (*a*) Adjusted R^2 values from linear regression models predicting the fractional cover of each grass lineage within 1 m^2 AOP pixels using MESMA estimates, incorporating subfamily as an additional covariate (MESMA prediction ~ observed % cover + subfamily) and a bareground endmember. (*b*) The table presents the differences between models that include subfamily as a covariate and those that do not. Improvements in model fits with the addition of subfamily as a covariate are indicated by negative RMSE (i.e. a reduction in error) and positive R^2 values (i.e. an increase in variance explained). The models evaluate the effectiveness of endmembers derived at both the plot and leaf levels. All results are statistically significant with $p < 0.000$.

	Leaf-level focal		Leaf-level all		Plot-level focal		Plot-level All	
Site	R^2	RMSE	R^2	RMSE	R^2	RMSE	R^2	RMSE
KONZ	0.67	15.94	0.72	15.39	0.87	16.46	0.96	9.44
CPER	0.33	14.91	0.18	17.30	0.60	18.60	0.48	22.52
WOOD	0.07	11.49	0.34	12.30	0.50	17.21	0.07	11.49
CCR	0.42	19.76	0.48	17.87	0.53	26.59	0.48	17.87
(b)								
Site	Diff R^2	Diff RMSE	Diff R^2	Diff RMSE	Diff R^2	Diff RMSE	Diff R^2	Diff RMSE
KONZ	0.33	−6.53	0.35	−7.62	0.43	−17.23	0.46	−23.23
CPER	0.16	−1.74	0.09	−0.92	0.60	−10.84	0.46	−8.31
WOOD	0.08	−0.47	0.34	−2.80	0.28	−4.35	0.08	−0.47
CCR	0.27	−4.07	0.35	−5.30	0.52	−12.05	0.35	−5.30

RMSE of 12.30 and an R^2 of 0.34 using leaf-level endmembers from all sites when subfamily was included and had a RMSE of 15.10 and an R^2 of 0 when subfamily was omitted. CCR had the highest RMSE of 17.87 and an R^2 of 0.48, and an RMSE of 23.17 and an R^2 of 0.13 when the subfamily was not included. Overall, KONZA consistently achieved the highest R^2 values across all approaches, while WOOD had the lowest R^2 except when applying the leaf-level endmembers from all sites. The inclusion of subfamily as a covariate was always significant ($p \leq 0.01$) and increased R^2 by 0.32 on average, but was as high as 0.60, for each approach across all sites and lowered the RMSE on average by 6.95, but as high as 23.23, underscoring the importance of subfamily identity in improving predictive accuracy of grassland composition.

3.2. Classification of dominant lineages

3.2.1. Leaf-level endmembers

When using only validation plots that had a lineage present at 30% cover or higher (which excluded the bareground class as bareground did not exceed 30%), the number of plots went from 430 to 297; however, accuracies generally improved compared to models that did not use a threshold of minimum percent cover. Using leaf-level endmembers measured from only the focal site, the overall prediction accuracy reached 90.3% with an MCC of 0.84 (Figure 3(a)). The accuracies for each individual lineage were all 75% or higher (diagonals in Figure 3(a)). Panicoideae had the lowest classification accuracy with misclassifications into Andropogoneae. When using leaf-level endmembers from all sites, the overall prediction accuracy reached 87.5% with an MCC of 0.77 (Figure 3(b)). The accuracies for each individual

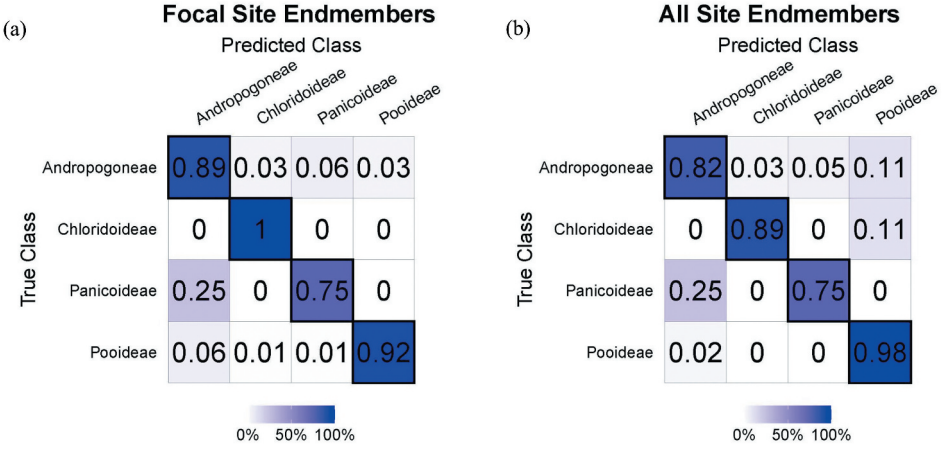

Figure 3. Mean normalised confusion matrices for MESMA classification of National Ecological Observatory Network (NEON) Airborne Observatory Platform (AOP) hyperspectral image pixels into the most dominant lineage using leaf-level endmembers from the focal site (a) and from all sites (b). Classification accuracy for each lineage is across the diagonal, and all other cells in the matrix describe the error rate. Using endmembers from focal sites resulted in an overall accuracy of 90.3% with an MCC of 0.84. Using endmembers across all sites resulted in an overall accuracy of 87.5% with an MCC of 0.80.

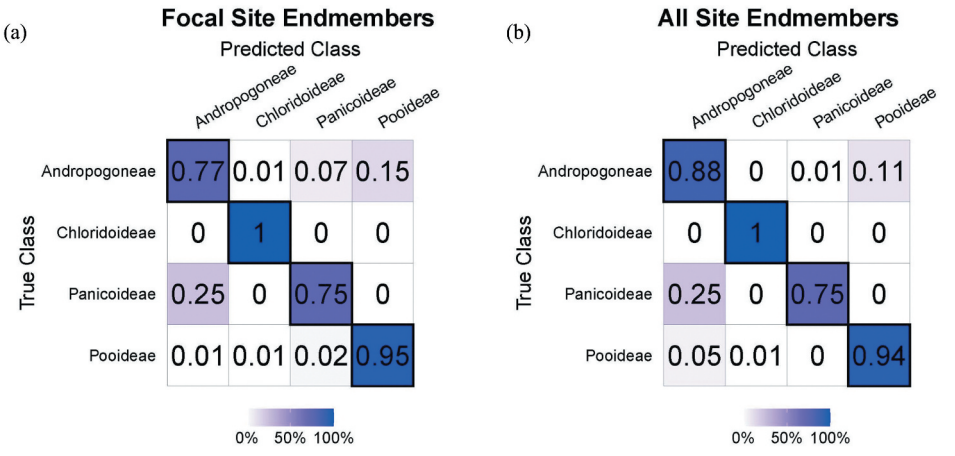

Figure 4. Mean normalised confusion matrices for MESMA classification of National Ecological Observatory Network (NEON) Airborne Observatory Platform (AOP) hyperspectral image using plot-level endmembers from the focal site (a) and from all sites (b). *Classification accuracy for each lineage is across the diagonal, and all other cells on the matrix describe the error rate. Using endmembers from focal sites only resulted in an overall accuracy of 85.1% with an MCC of 0.75. Using endmembers across all sites resulted in an overall accuracy of 90.7% with an MCC of 0.84.*

lineage were all 75% or higher, again with Panicoideae having the lowest classification accuracy of 75% (diagonals in Figure 3(b)), with misclassifications into Andropogoneae. Overall model accuracies include bareground endmembers, however when using a 30% cover threshold, bareground was never misclassified as a grass lineage. Therefore, confusion matrices (Figure 3(a,b)) are normalized to only show lineage classification/misclassification.

3.2.2. Plot-level endmembers

Using plot-level endmembers from a focal site to classify the most dominant lineage (i.e. the lineage with the highest percent cover, with a minimum cover of at least 30%), the overall prediction accuracy was 85.1% with an MCC of 0.77 (Figure 4(a)). The individual lineages Chloridoideae and Pooideae had accuracies over 95%, while Andropogoneae and Panicoideae had accuracies over 75% (diagonals in Figure 4(a)). The presence of Panicoideae tended to be confused for Andropogoneae. Using the plot-level endmember with a 30% threshold on percent cover from all sites, the overall prediction accuracy reached 90.7% with an MCC of 0.84 (Figure 4(b)). Andropogoneae, Chloridoideae, and Pooideae had individual accuracies over 87%, while Panicoideae had an accuracy of 75% (diagonals in Figure 4(b)). Panicoideae were misclassified as Andropogoneae. Similarly, to the leaf-level endmember models, overall model accuracies include bareground endmembers; however, when using a 30% cover threshold, bareground was never misclassified as a grass lineage. Therefore, confusion matrices (Figure 4(a,b)) are normalized to only show lineage classification/misclassification.

4. Discussion

To predict the future functionality of grassland ecosystems accurately, it is crucial to understand the distribution patterns of dominant functional types (Gholizadeh et al. 2022; Griffith et al. 2020; Still, Cotton, and Griffith 2019). Grassland ecosystems typically consist of heterogeneous assemblages of species at fine scales. Mapping the distribution of grasses using imagery often necessitates working with mixed pixels, which can introduce uncertainty. This is because of a scale mismatch between the small size of plant species found in grasslands in relation to the spatial resolution of imagery (Gamon et al. 2020; Gholizadeh et al. 2022). To assess the potential for spectral unmixing techniques to classify grassland composition at fine scales, we disaggregated 1-m NEON AOP hyperspectral pixels using MESMA and compared the effectiveness of leaf vs. plot-level endmembers in addition to the transferability of endmembers across sites. In general, the four endmember approaches we used to detect the dominant grass lineages at varying sites resulted in similarly high accuracies (~85–90%). However, the use of leaf-level spectral endmembers from focal sites compared to aggregating spectra across all sites resulted in slightly higher overall accuracies, while the use of plot-level spectral endmembers from all sites had slightly higher overall accuracies than using endmembers from the focal site.

Leaf traits, which influence leaf-level reflectance, may vary more across sites (e.g. Pau et al. 2025) compared to structural traits, which influence plot-level reflectance. Canopy structure, leaf area, and leaf angle may differ less across species and sites, and therefore serve as representative endmembers even across sites for particular lineages. For instance, the canopy trait, LAI, which is the total leaf area relative to the ground area, influences the proportion of light absorbed or reflected by a canopy versus other components like soil. Higher LAI generally increases reflectance in certain bands, especially in the near-infrared region, which is sensitive to vegetation (Shibayama and Akiyama 1989; Turner et al. 1999). Similarly, leaf size and leaf angle distribution of grass lineages, which can affect the amount and directionality of reflected light, may differ less across species and sites (Supplementary Materials Figure S4).

Our work further demonstrates the importance of taxonomic identity rather than measures of diversity per se. When unmixing NEON AOP pixels, our results highlight the advantage of incorporating phylogenetic information for predicting grassland composition, which substantially improved predictive accuracies (Table 3(b)). In other words, the fractional cover of pixels dominated by certain lineages was better predicted than others, suggesting that particular traits associated with lineage have a stronger spectral signal. This result was consistent when using endmembers at the leaf-level and at the plot-level from both the focal site and across all sites with at least a 30% threshold. Relevant traits may propagate across scales or there are both leaf and canopy traits associated with lineages that have strong optical properties. More specifically, sites dominated by Andropogoneae, i.e. KONZ and CCR, tended to have higher accuracies for predicting fractional cover. Additionally, these two sites also had the lowest bareground presence. While the presence of bareground did not affect classifications using a dominance threshold, when a threshold was not applied the presence of bareground in small proportions also played a role in predictive accuracies for fractional abundance of the dominant grass lineages in the pixel (Figure S2 and S3).

Although we generally achieved high classification accuracy, spectral similarity among vegetation types may have caused classification errors, which can lead to confusion between functionally or structurally similar plant lineages. This challenge is particularly pronounced in classifying our Panicoideae group, which tended to be misclassified as Andropogoneae, a tribe within the subfamily Panicoideae. Because these two groups share a close evolutionary relationship, they likely share similar traits and thus similar spectral signatures (Slapikas et al. 2024; Pau et al. 2025). Andropogoneae is nonetheless an ecologically distinct group with unique functional traits that differentiate it from other Panicoideae (Donnelly et al. 2023; Griffith et al. 2020). While Andropogoneae were classified with high accuracy, the larger Panicoideae group may lack distinctiveness and exhibit larger variability in their spectral signatures (Figure 3 and 4). On the other hand, Chloridoideae was classified with almost perfect accuracy in dominance classifications because it tends to not co-occur with other lineages or with only Pooideae, and it has a very distinct spectral signature (Figure 2).

Another potential reason for classification errors is geolocational misalignment between our validation plots and imagery (Pau et al. 2020). Even with our high (1–3 m) GPS accuracies recorded for our field plots, georectification and mosaicking of image flight lines can result in pixel shifts. Radiance from neighbouring pixels can also affect the focal pixel (Inamdar et al. 2020), particularly with 1 m^2 pixels provided by the NEON AOP. This may have contributed to sometimes low prediction accuracy for some sites and some lineages. Konza Prairie, the site with the highest R^2 when predicting fractional cover, generally has low turnover of lineages at scales <10 m and also had no recorded bare-ground in transects, which contributed to its successful classification.

Not surprisingly, predicting dominant lineages (30% cover or greater) resulted in higher predicted accuracies than fractional cover. Previous studies (e.g. Chen et al. 2018; Lopatin et al. 2017) found that classifications of grassland composition at the species level have limitations due to inter-species spectral signal mixing. Our results suggest that spectral distinctiveness may be relatively less important than spatial coverage given that classification of dominance was more successful than fractional coverage. Mapping dominant species and lineages should help link patterns of diversity to ecosystem functions and help predict future patterns of global change at relevant spatial scales (Avolio et al. 2019; Pau and Dee 2016).

Overall, our results show strong potential for modelling the distribution of grass lineages at fine scales using hyperspectral imagery. We found that leaf-level spectra contain high information content for discriminating grass evolutionary lineages as seen in Figures 3 and 5. Our work demonstrates that using leaf endmember collections, rather than more time-consuming plot-based endmembers, can lead to comparably high predictive accuracies. However, plot-level spectra appear more transferable across sites and suggest that canopy-level traits may be more robust to environmental differences. Our work also shows that using plot spectra from already existing spectral libraries may be appropriate to apply to new sites. In all cases, our models predicted some lineages with greater accuracy than others. Partitioning the large Panicoideae subfamily further could help to improve model accuracy. Given the increasing number of existing and near-future hyperspectral satellite missions (e.g. CHIME, SBG, EnMAP), our approach can be scaled to spaceborne imaging spectrometers by resampling the leaf and plot spectral libraries to each sensor's capabilities, providing potentially global grassland plant

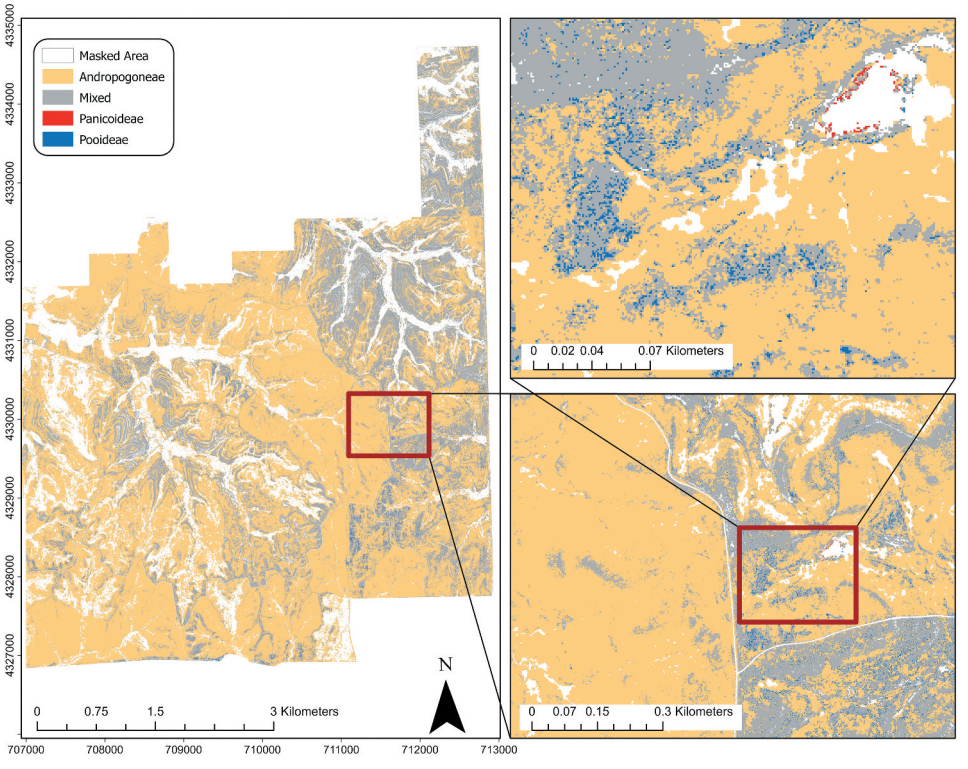

Figure 5. The far-left image is a classified map depicting the spatial distribution of dominant grass lineages (Andropogoneae, Chloridoideae, Panicoideae, and Pooideae) at the Konza Prairie Biological Station, derived from leaf-level endmembers from Konza only (i.e., the focal site) using MESMA applied to NEON AOP hyperspectral imagery at 1 m2 spatial resolution. The bottom right image highlights two distinct regions: the left side is dominated by Andropogoneae (yellow) and are areas with frequent fire and no grazers; the right side shows more mixed regions (grey) and are areas with fire and grazing treatments where species richness tends to be higher and multiple lineages coexist. Many of the mixed pixels in these regions include the presence of Chloridoideae. The top right image is a further magnified view of the image below, illustrating the fine-scale spatial distribution of each lineage as classified from the hyperspectral data. Regions in white are tree or shrub dominated and masked based on the NEON CHM (see Methods).

diversity maps and long-term monitoring. To improve the accuracy of detecting grass evolutionary lineages, future research should explore the use of multiple classification approaches instead of relying on a single method. Different classifiers can complement each other by handling different sources of error in spectral unmixing. Some studies suggest using a discriminative classification model (Support Vector Machines, Random Forest, Gradient Boosting Machines, or Artificial Neural Networks) alongside spectral unmixing. In this approach, if spectral unmixing struggles to classify a pixel with confidence, the system would instead rely on the discriminative classification model to make the decision, and vice versa (Li et al. 2015). By mapping and modelling the distribution of grass evolutionary lineages, we can better understand the environmental factors that shape their

distributions and help monitor how distributions might shift in response to climate change or land use changes.

Acknowledgements

This research was supported by the National Science Foundation (NSF) and the National Ecological Observatory Network (NEON), a programme funded by the NSF and operated under a cooperative agreement with Battelle Memorial Institute. We sincerely thank the site managers at Konza Prairie, Colorado Plains Experimental Range, Chase Lake National Wildlife Refuge, and Cedar Creek Ecosystem Reserve for their invaluable support and access to field sites. Additionally, we acknowledge funding from NSF award 1926108, which supported contributions from SP and RS and 1926345, which supported JBN and RD. We extend our gratitude to Daniel Griffith for his invaluable assistance in species identification and Christopher Still, Che-Ling Ho, Brent Helliker, and Adam Abdullahi for their assistance with field surveying.

Disclosure statement

No potential conflict of interest was reported by the author(s).

Funding

The work was supported by the National Science Foundation [1926108,1926345].

ORCID

Ryan Slapikas http://orcid.org/0000-0002-6975-2169
Ryan C. Donnelly http://orcid.org/0000-0003-4628-2376

Data availability statement

All data used for the creation of this manuscript are published on GitHub and available at Zenodo DOI 10.5281/zenodo.15186274. Figures were made with 'ggplot2' version 3.3.6 (Wickham 2016). Maps were created using 'tmap' version 3.3-3 (Tennekes 2018). Part of the software used with this manuscript for the calculation and jump correction is licenced under MIT and published on GitHub https://github.com/EnSpec/SpecDAL.

References

Adams, J. B., M. O. Smith, and P. E. Johnson. 1986. "Spectral Mixture Modeling: A New Analysis of Rock and Soil Types at the Viking Lander 1 Site." *Journal of Geophysical Research Solid Earth* 91 (B8): 8098–8112. https://doi.org/10.1029/JB091iB08p08098.

Ali, I., F. Cawkwell, E. Dwyer, B. Barrett, and S. Green. 2016. "Satellite Remote Sensing of Grasslands: From Observation to Management." *Journal of Plant Ecology* 9 (6): 649–671. https://doi.org/10.1093/jpe/rtw005.

Anderegg, L. D. L., D. M. Griffith, J. Cavender-Bares, W. J. Riley, J. A. Berry, T. E. Dawson, and C. J. Still. 2022. "Representing Plant Diversity in Land Models: An Evolutionary Approach to Make "Functional Types" More Functional." *Global Change Biology* 28 (8): 2541–2554. https://doi.org/10.1111/gcb.16040.

Asner, G. P., and K. B. Heidebrecht. 2002. "Spectral Unmixing of Vegetation, Soil and Dry Carbon Cover in Arid Regions: Comparing Multispectral and Hyperspectral Observations." *International Journal of Remote Sensing* 23 (19): 3939–3958. https://doi.org/10.1080/01431160110115960.

Asner, G. P., and R. E. Martin. 2011. "Canopy Phylogenetic, Chemical and Spectral Assembly in a Lowland Amazonian Forest." *New Phytologist* 189 (4): 999–1012. https://doi.org/10.1111/j.1469-8137.2010.03549.x.

Avolio, M. L., E. J. Forrestel, C. C. Chang, K. J. La Pierre, K. T. Burghardt, and M. D. Smith. 2019. "Demystifying Dominant Species." *New Phytologist* 223 (3): 1106–1126. https://doi.org/10.1111/nph.15789.

Boardman, J. W., F. A. Kruse, and R. O. Green. 1995. "Mapping Target Signatures via Partial Unmixing of AVIRIS Data." In *Summaries of the Fifth Annual JPL Airborne Earth Science Workshop*, Vol. 1. AVIRIS workshop.

Chang, C. I., C. C. Wu, and H. M. Chen. 2009. "Random Pixel Purity Index." *IEEE Geoscience & Remote Sensing Letters* 7 (2): 324–328. https://doi.org/10.1109/LGRS.2009.2034610.

Chen, X., D. Wang, J. Chen, C. Wang, and M. Shen. 2018. "The Mixed Pixel Effect in Land Surface Phenology: A Simulation Study." *Remote Sensing of Environment* 211:338–344. https://doi.org/10.1016/j.rse.2018.04.030.

Chlus, A. 2023. "HyTools (1.5.0) [Python]." Environmental Spectroscopy Lab. https://github.com/EnSpec/HyTools.

Donnelly, R. C., E. R. Wedel, J. H. Taylor, J. B. Nippert, B. R. Helliker, W. J. Riley, C. J. Still, and D. M. Griffith. 2023. "Evolutionary Lineage Explains Trait Variation Among 75 Coexisting Grass Species." *New Phytologist* 239 (3): 875–887. https://doi.org/10.1111/nph.18983.

Dorigo, W., M. Bachmann, and W. Heldens. 2006. *AS Toolbox and Processing of Field Spectra User's Manual*. Institute for Environment and Geo-Information, German Aerospace Center (DLR). https://vdocuments.mx/as-toolbox-processing-of-field-1go-to-envi-spectral-libraries-spectral-library.html?page=1 .

Fernández-Guisuraga, J. M., L. Calvo, and S. Suárez-Seoane. 2020. "Comparison of Pixel Unmixing Models in the Evaluation of Post-Fire Forest Resilience Based on Temporal Series of Satellite Imagery at Moderate and Very High Spatial Resolution." *ISPRS Journal of Photogrammetry & Remote Sensing* 164:217–228. https://doi.org/10.1016/j.isprsjprs.2020.05.004.

Fernández-Manso, A., C. Quintano, and D. Roberts. 2012. "Evaluation of Potential of Multiple Endmember Spectral Mixture Analysis (MESMA) for Surface Coal Mining Affected Area Mapping in Different World Forest Ecosystems." *Remote Sensing of Environment* 127:181–193. https://doi.org/10.1016/j.rse.2012.08.028.

Foody, G. M. 2020. "Explaining the Unsuitability of the Kappa Coefficient in the Assessment and Comparison of the Accuracy of Thematic Maps Obtained by Image Classification." *Remote Sensing of Environment* 239:111630. https://doi.org/10.1016/j.rse.2019.111630.

Franc, V., V. Hlaváč, and M. Navara. 2005. "Sequential Coordinate-Wise Algorithm for the Non-Negative Least Squares Problem." International conference on computer analysis of images and patterns, Berlin, Heidelberg: 407–414. Springer. https://doi.org/10.1007/11556121_50.

Gamon, J. A., R. Wang, H. Gholizadeh, B. Zutta, P. A. Townsend, and J. Cavender-Bares. 2020. "Consideration of Scale in Remote Sensing of Biodiversity." In *Remote Sensing of Plant Biodiversity*, 425–447. Cham: Springer International Publishing.

Gholizadeh, H., A. P. Dixon, K. H. Pan, N. A. McMillan, R. G. Hamilton, S. D. Fuhlendorf, J. A. Gamon, and J. A. Gamon. 2022. "Using Airborne and DESIS Imaging Spectroscopy to Map Plant Diversity Across the Largest Contiguous Tract of Tallgrass Prairie on Earth." *Remote Sensing of Environment* 281:113254. https://doi.org/10.1016/j.rse.2022.113254.

Gholizadeh, H., J. A. Gamon, P. A. Townsend, A. I. Zygielbaum, C. J. Helzer, G. Y. Hmimina, R. Yu, R. M. Moore, A. K. Schweiger, and J. Cavender-Bares. 2019. "Detecting Prairie Biodiversity with Airborne Remote Sensing." *Remote Sensing of Environment* 221:38–49. https://doi.org/10.1016/j.rse.2018.10.037.

Gholizadeh, H., J. A. Gamon, A. I. Zygielbaum, R. Wang, A. K. Schweiger, and J. Cavender-Bares. 2018. "Remote Sensing of Biodiversity: Soil Correction and Data Dimension Reduction Methods

Improve Assessment of α-Diversity (Species Richness) in Prairie Ecosystems." *Remote Sensing of Environment* 206:240–253. https://doi.org/10.1016/j.rse.2017.12.014.

Gong, P., and A. Zhang. 1999. "Noise Effect on Linear Spectral Unmixing." *Geographic Information Sciences* 5 (1): 52–57. https://doi.org/10.1080/10824009909480514.

Goodin, D. G., J. Gao, and G. M. Henebry. 2004. "The Effect of Solar Illumination Angle and Sensor View Angle on Observed Patterns of Spatial Structure in Tallgrass Prairie." *IEEE Transactions on Geoscience & Remote Sensing* 42 (1): 154–165. https://doi.org/10.1109/TGRS.2003.815674.

Griffith, D. M., C. P. Osborne, E. J. Edwards, S. Bachle, D. J. Beerling, W. J. Bond, C. J. Still, et al. 2020. "Lineage-Based Functional Types: Characterising Functional Diversity to Enhance the Representation of Ecological Behaviour in Land Surface Models." *New Phytologist* 228 (1): 15–23. https://doi.org/10.1111/nph.16773.

Guerini Filho, M., T. M. Kuplich, and F. L. D. Quadros. 2020. "Estimating Natural Grassland Biomass by Vegetation Indices Using Sentinel 2 Remote Sensing Data." *International Journal of Remote Sensing* 41 (8): 2861–2876. https://doi.org/10.1080/01431161.2019.1697004.

He, Y., X. Guo, and J. Wilmshurst. 2006. "Studying Mixed Grassland Ecosystems I: Suitable Hyperspectral Vegetation Indices." *Canadian Journal of Remote Sensing* 32 (2): 98–107. https://doi.org/10.5589/m06-009.

Hellmann, C., A. Große-Stoltenberg, V. Lauströ, J. Oldeland, and C. Werner. 2015. "Retrieving Nitrogen Isotopic Signatures from Fresh Leaf Reflectance Spectra: Disentangling δ15n from Biochemical and Structural Leaf Properties." *Frontiers in Plant Science* 6. https://doi.org/10.3389/fpls.2015.00307.

Hicke, J. A., G. P. Asner, J. T. Randerson, C. Tucker, S. Los, R. Birdsey, J. C. Jenkins, and C. Field. 2002. "Trends in North American Net Primary Productivity Derived from Satellite Observations, 1982–1998." *Global Biogeochemical Cycles* 16 (2): 2–1–2–14. https://doi.org/10.1029/2001GB001550.

Inamdar, D., M. Kalacska, G. Leblanc, and J. P. Arroyo-Mora. 2020. "Characterizing and Mitigating Sensor Generated Spatial Correlations in Airborne Hyperspectral Imaging Data." *Remote Sensing* 12 (4): 641. https://doi.org/10.3390/rs12040641.

Jacquemoud, S., F. Baret, and J. F. Hanocq. 1992. "Modeling Spectral and Bidirectional Soil Reflectance." *Remote Sensing of Environment* 41 (2–3): 123–132. https://doi.org/10.1016/0034-4257(92)90072-R.

Kampe, T. U., B. R. Johnson, M. A. Kuester, and M. Keller. 2010. "NEON: The First Continental-Scale Ecological Observatory with Airborne Remote Sensing of Vegetation Canopy Biochemistry and Structure." *Journal of Applied Remote Sensing* 4 (1): 043510. https://doi.org/10.1117/1.3361375.

Kothari, S., and A. K. Schweiger. 2022. "Plant Spectra as Integrative Measures of Plant Phenotypes." *The Journal of Ecology* 110 (11): 2536–2554. https://doi.org/10.1111/1365-2745.13972.

Kuemmerle, T., A. Röder, and J. Hill. 2006. "Separating Grassland and Shrub Vegetation by Multidate Pixel-Adaptive Spectral Mixture Analysis." *International Journal of Remote Sensing* 27 (15): 3251–3271. https://doi.org/10.1080/01431160500488944.

Lehmann, C. E. R., D. M. Griffith, K. J. Simpson, T. M. Anderson, S. Archibald, D. J. Beerling, W. J. Bond, et al. 2019. "Functional Diversification Enabled Grassy Biomes to Fill Global Climate Space." *bioRxiv*. https://doi.org/10.1016/j.jaridenv.2004.11.004.

Lehnert, L. W., H. Meyer, W. A. Obermeier, B. Silva, B. Regeling, and J. Bendix. 2019. "Hyperspectral Data Analysis in R: The hsdar Package." *Journal of Statistical Software* 89 (12): 1–23. https://doi.org/10.18637/jss.v089.i12.

Li, X., X. Jia, and L. Wang, & K. Zhao. 2015. "On Spectral Unmixing Resolution Using Extended Support Vector Machines." *IEEE Transactions on Geoscience and Remote Sensing* 53 (9): 4985–4996.

Lopatin, J., F. E. Fassnacht, T. Kattenborn, and S. Schmidtlein. 2017. "Mapping Plant Species in Mixed Grassland Communities Using Close Range Imaging Spectroscopy." *Remote Sensing of Environment* 201:12–23. https://doi.org/10.1016/j.rse.2017.08.031.

Olofsson, P., R. Gilmore, and M. Millones. 2011. "Death to Kappa: Birth of Quantity Disagreement and Allocation Disagreement for Accuracy Assessment." *International Journal of Remote Sensing* 32 (15): 4407–4429. https://doi.org/10.1080/01431161.2011.552923.

Paruelo, J. M., and W. K. Lauenroth. 1996. "Relative Abundance of Plant Functional Types in Grasslands and Shrublands of North America." *Ecological Applications* 6 (4): 1212–1224. https://doi.org/10.2307/2269602.

Pau, S., and L. E. Dee. 2016. "Remote Sensing of Species Dominance and the Value for Quantifying Ecosystem Services." *Remote Sensing in Ecology and Conservation* 2 (3): 141–151. https://doi.org/10.1002/rse2.23.

Pau, S., J. B. Nippert, R. Slapikas, D. Griffith, S. Bachle, B. R. Helliker, R. C. O'Connor, W. J. Riley, C. J. Still, and M. Zaricor. 2022. "Poor Relationships Between NEON Airborne Observation Platform Data and Field-Based Vegetation Traits at a Mesic Grassland." *Ecology* 103 (2): e03590. https://doi.org/10.1002/ecy.3590.

Pau, S., R. Slapikas, C. L. Ho, S. L. Bayliss, R. C. Donnelly, A. Abdullahi, B. R. Helliker, et al. 2025. "Hyperspectral Leaf Reflectance of Grasses Varies with Evolutionary Lineage More Than with Site." *Ecosphere* 16 (4): e70257. https://doi.org/10.1002/ecs2.70257 .

Pazúr, R., N. Huber, D. Weber, C. Ginzler, and B. Price. 2022. "A National Extent Map of Cropland and Grassland for Switzerland Based on Sentinel-2 Data." *Earth System Science Data* 14 (1): 295–305. https://doi.org/10.5194/essd-14-295-2022.

Psomas, A., M. Kneubühler, S. Huber, K. Itten, and N. E. Zimmermann. 2011. "Hyperspectral Remote Sensing for Estimating Aboveground Biomass and for Exploring Species Richness Patterns of Grassland Habitats." *International Journal of Remote Sensing* 32 (24): 9007–9031. https://doi.org/10.1080/01431161.2010.532172.

Radeloff, V. C., D. J. Mladenoff, and M. S. Boyce. 1999. "Detecting Jack Pine Budworm Defoliation Using Spectral Mixture Analysis: Separating Effects from Determinants." *Remote Sensing of Environment* 69 (2): 156–169. https://doi.org/10.1016/S0034-4257(99)00008-5.

Ranson, K. J., C. S. T. Daughtry, L. L. Biehl, and M. E. Bauer. 1985. "Sun-View Angle Effects on Reflectance Factors of Corn Canopies." *Remote Sensing of Environment* 18 (2): 147–161. https://doi.org/10.1016/0034-4257(85)90045-8.

Rashed, T., J. R. Weeks, D. Roberts, J. Rogan, and R. Powell. 2003. "Measuring the Physical Composition of Urban Morphology Using Multiple Endmember Spectral Mixture Models." *Photogrammetric Engineering & Remote Sensing* 69 (9): 1011–1020. https://doi.org/10.14358/PERS.69.9.1011.

Roberts, D. A., M. Gardner, R. Church, S. Ustin, G. Scheer, and R. O. Green. 1998. "Mapping Chaparral in the Santa Monica Mountains Using Multiple Endmember Spectral Mixture Models." *Remote Sensing of Environment* 65 (3): 267–279. https://doi.org/10.1016/S0034-4257(98)00037-6.

Roberts, D. A., M. O. Smith, D. E. Sabol, J. B. Adams, and S. L. Ustin. 1992. "Mapping the Spectral Variability in Photosynthetic and Non-Photosynthetic Vegetation, Soils, and Shade Using AVIRIS." https://ntrs.nasa.gov/citations/19940012206.

Rossi, C., and H. Gholizadeh. 2023. "Uncovering the Hidden: Leveraging Sub-Pixel Spectral Diversity to Estimate Plant Diversity from Space." *Remote Sensing of Environment* 296:113734. https://doi.org/10.1016/j.rse.2023.113734.

Shibayama, M., and T. Akiyama. 1989. "Seasonal Visible, Near-Infrared and Mid-Infrared Spectra of Rice Canopies in Relation to LAI and Above-Ground Dry Phytomass." *Remote Sensing of Environment* 27 (2): 119–127. https://doi.org/10.1016/0034-4257(89)90011-4.

Slapikas, R., S. Pau, R. C. Donnelly, C.-L. Ho, J. B. Nippert, B. R. Helliker, W. J. Riley, C. J. Still, and D. M. Griffith. 2024. "Grass Evolutionary Lineages Can Be Identified Using Hyperspectral Leaf Reflectance." *Journal of Geophysical Research Biogeosciences* 129 (2): e2023JG007852. https://doi.org/10.1029/2023JG007852.

Smit, H. J., M. J. Metzger, and F. Ewert. 2008. "Spatial Distribution of Grassland Productivity and Land Use in Europe." *Agricultural Systems* 98 (3): 208–219. https://doi.org/10.1016/j.agsy.2008.07.004.

Smith, M. O., S. L. Ustin, J. B. Adams, and A. R. Gillespie. 1990. "Vegetation in Deserts: I. A Regional Measure of Abundance from Multispectral Images." *Remote Sensing of Environment* 31 (1): 1–26. https://doi.org/10.1016/0034-4257(90)90074-V.

Somers, B., G. P. Asner, L. Tits, and P. Coppin. 2011. "Endmember Variability in Spectral Mixture Analysis: A Review." *Remote Sensing of Environment* 115 (7): 1603–1616. https://doi.org/10.1016/j.rse.2011.03.003.

Song, C. 2005. "Spectral Mixture Analysis for Subpixel Vegetation Fractions in the Urban Environment: How to Incorporate Endmember Variability?" *Remote Sensing of Environment* 95 (2): 248–263. https://doi.org/10.1016/j.rse.2005.01.002.

Still, C. J., J. A. Berry, G. J. Collatz, and R. S. DeFries. 2003. "Global Distribution of C3 and C4 Vegetation: Carbon Cycle Implications." *Global Biogeochemical Cycles* 17 (1): 6–1–6–14. https://doi.org/10.1029/2001GB001807.

Still, C. J., J. M. Cotton, and D. M. Griffith. 2019. "Assessing Earth System Model Predictions of C4 Grass Cover in North America: From the Glacial Era to the End of This Century." *Global Ecology & Biogeography* 28 (2): 145–157. https://doi.org/10.1111/geb.12830.

Tennekes, M. 2018. "Tmap: Thematic Maps in R [software]." *Journal of Statistical Software* 84 (6): 1–39. https://doi.org/10.18637/jss.v084.i06.

Tompkins, S., J. F. Mustard, C. M. Pieters, and D. W. Forsyth. 1997. "Optimization of Endmembers for Spectral Mixture Analysis." *Remote Sensing of Environment* 59 (3): 472–489. https://doi.org/10.1016/S0034-4257(96)00122-8.

Turner, D. P., W. B. Cohen, R. E. Kennedy, K. S. Fassnacht, and J. M. Briggs. 1999. "Relationships Between Leaf Area Index and Landsat TM Spectral Vegetation Indices Across Three Temperate Zone Sites." *Remote Sensing of Environment* 70 (1): 52–68. https://doi.org/10.1016/S0034-4257(99)00057-7.

Van Cleemput, E., P. Adler, and K. N. Suding. 2023. "Making Remote Sense of Biodiversity: What Grassland Characteristics Make Spectral Diversity a Good Proxy for Taxonomic Diversity?" *Global Ecology & Biogeography* 32 (12): 2177–2188. https://doi.org/10.1111/geb.13759.

Van Cleemput, E., L. Vanierschot, B. Fernández-Castilla, O. Honnay, and B. Somers. 2018. "The Functional Characterization of Grass-and Shrubland Ecosystems Using Hyperspectral Remote Sensing: Trends, Accuracy and Moderating Variables." *Remote Sensing of Environment* 209:747–763. https://doi.org/10.1016/j.rse.2018.02.030.

Wessman, C. A., C. A. Bateson, and T. L. Benning. 1997. "Detecting Fire and Grazing Patterns in Tallgrass Prairie Using Spectral Mixture Analysis." *Ecological Applications* 7 (2): 493–511. https://doi.org/10.1890/1051-0761(1997)007[0493:DFAGPI]2.0.CO;2.

Wickham, H. 2016. "ggplot2: Elegant graphics for data analysis." Springer-Verlag New York. [Software] https://ggplot2.tidyverse.org.

Wilson, J. B., R. K. Peet, J. Dengler, and M. Pärtel. 2012. "Plant Species Richness: The World Records." *Journal of Vegetation Science* 23 (4): 796–802. https://doi.org/10.1111/j.1654-1103.2012.01400.x.

Wu, C., and A. T. Murray. 2003. "Estimating Impervious Surface Distribution by Spectral Mixture Analysis." *Remote Sensing of Environment* 84 (4): 493–505. https://doi.org/10.1016/S0034-4257(02)00136-0.

Wu, J., Y. Li, B. Zhong, Q. Liu, S. Wu, C. Ji, J. Zhao, L. Li, X. Shi, and A. Yang. 2023. "Integrated Vegetation Cover of Typical Steppe in China Based on Mixed Decomposing Derived from High Resolution Remote Sensing Data." *Science of the Total Environment* 904:166738. https://doi.org/10.1016/j.scitotenv.2023.166738.

Xu, B., X. C. Yang, W. G. Tao, Z. H. Qin, H. Q. Liu, J. M. Miao, and Y. Y. Bi. 2008. "MODIS-Based Remote Sensing Monitoring of Grass Production in China." *International Journal of Remote Sensing* 29 (17–18): 5313–5327. https://doi.org/10.1080/01431160802036276.